

Simulation of Fermionic and Bosonic Critical Points with Emergent SO(5) Symmetry

Toshihiro Sato,¹ Zhenjiu Wang,² Yuhai Liu,³ Disha Hou,⁴
Martin Hohenadler,^{1,5} Wenan Guo,^{4,6} and Fakher F. Assaad^{1,7}¹*Institut für Theoretische Physik und Astrophysik, Universität Würzburg, 97074 Würzburg, Germany*²*Max-Planck-Institut für Physik komplexer Systeme, Dresden 01187, Germany*³*School of Science, Beijing University of Posts and Telecommunications, Beijing 100876, China*⁴*Department of Physics, Beijing Normal University, Beijing 100875, China*⁵*Independent Researcher, Josef-Retzer-Str. 7, 81241 Munich, Germany*⁶*Beijing Computational Science Research Center, 10 East Xibeiwang Road, Beijing 100193, China*⁷*Würzburg-Dresden Cluster of Excellence ct.qmat, Am Hubland, 97074 Würzburg, Germany*

We introduce a model of Dirac fermions in 2+1 dimensions with a semimetallic, a quantum spin-Hall insulating (QSHI), and an s-wave superconducting (SSC) phase. The phase diagram features a multicritical point at which all three phases meet as well as a QSHI-SSC deconfined critical point. The QSHI and SSC orders correspond to mutually anti-commuting mass terms of the Dirac Hamiltonian. Based on this algebraic property, SO(5) symmetric field theories have been put forward to describe both types of critical points. Using quantum Monte Carlo simulations, we directly study the operator that rotates between QSHI and SSC states. The results suggest that it commutes with the low-energy effective Hamiltonian at criticality but has a gap in the ordered phases. This implies an emergent SO(5) symmetry at both the multicritical and the deconfined critical points.

Introduction.—Within the renormalization group theory of phase transitions [1], criticality is defined by scale invariance and operators are classified as either relevant, marginal, or irrelevant. The concept of an emergent symmetry refers to critical points that have a higher symmetry than the corresponding ultraviolet (UV) model as a result of the irrelevance of operators that break said symmetry. For instance, in interacting one-dimensional (1D) systems described by 1+1D field theories, emergent Lorentz symmetry is the rule [2] and leads to the interchangeability of space and time. In 2+1D, O(N) nonlinear sigma models are robust only for $N < 3$ [3, 4] so that O(2) symmetry can emerge in a Z_4 invariant model [5]. In other cases, emergent symmetries allow to rotate one ordered state into another. For example, the SO(5) theory of high-temperature superconductivity [6] conjectured the unification of the d-wave superconducting and antiferromagnetic orders. Away from a critical point with emergent symmetry, the operator describing the above rotation acquires a gap and is expected to manifest itself as a resonance with specific quantum numbers in spectroscopy measurements.

Dirac systems are a fruitful platform to investigate emergent symmetries [7]. Let us consider the 2+1D case of four two-component Dirac fields relevant for graphene [8]. In this setting, one can define quintuplets of mutually anti-commuting mass terms of either two Kekulé and three antiferromagnetic masses or two s-wave superconducting (SSC) and three quantum spin-Hall insulator (QSHI) masses, respectively [9]. Each quintuplet can be associated with a 5D superspin order parameter [10]. Theories in which Dirac fermions couple symmetrically to the superspin have SO(5) symmetry [11]. However, UV models of interacting Dirac fermions generically do not. A key question is, therefore, if the symmetry emerges at

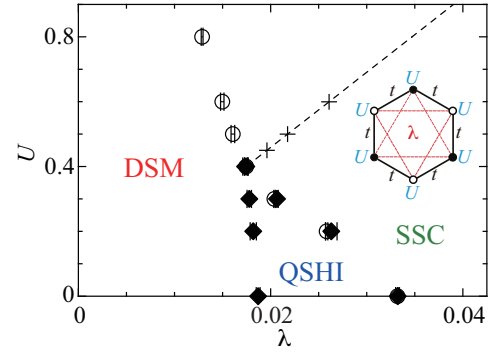


FIG. 1. Ground-state phase diagram with Dirac semimetal (DSM), quantum spin-Hall insulating (QSHI), and s-wave superconducting (SSC) phases from QMC simulations (see text). The dashed line and crosses indicate the values of g (0, 0.05, 0.1, 0.2) used in Fig. 3(b). Inset: honeycomb plaquette illustrating the hopping and interaction terms in Eq. (1).

critical points, of which we consider two classes. First, Gross-Neveu fermionic critical points [12] at which the superspin vector vanishes and which separate a Dirac semimetal (DSM) from an ordered phase (e.g., the DSM-QSHI and DSM-SSC transitions in Fig. 1). For this case, results from an ϵ -expansion [7] predict an emergent SO(5) symmetry. The second class are bosonic critical points, where amplitude fluctuations of the superspin can be neglected and the gapped fermions can be integrated out [13]. This case is described by an SO(5) symmetric nonlinear sigma model with a Wess-Zumino-Witten geometrical term, which has been suggested to describe deconfined quantum critical points (DQCPs) separating two phases with different order parameters [11, 14, 15].

In this Letter, we introduce and simulate a suitable lattice model. It has a global $SU(2) \times U(1)$ symmetry

associated with spin rotation symmetry and charge conservation, respectively. The model permits auxiliary-field quantum Monte Carlo (QMC) simulations without a sign problem and supports DSM, QSHI, and SSC phases, see Fig. 1. Based on measurements of the dynamics of the operator that rotates between QSHI and SSC states, we argue that $SO(5)$ symmetry indeed emerges both at a DSM-QSHI-SSC Gross-Neveu multicritical point and at QSHI-SSC DQCPs, at least at the intermediate energy scales accessible in our simulations.

Model and Method.—We consider the Hamiltonian

$$\hat{H} = -t \sum_{\langle i,j \rangle} (\hat{c}_i^\dagger \hat{c}_j + \text{H.c.}) - \lambda \sum_{\square} \left(\sum_{\langle\langle i,j \rangle\rangle \in \square} \hat{J}_{i,j} \right)^2 - U \sum_i \left(\hat{n}_{i\uparrow} - \frac{1}{2} \right) \left(\hat{n}_{i\downarrow} - \frac{1}{2} \right). \quad (1)$$

Here, $\hat{c}_{i\sigma}^\dagger$ ($\hat{c}_{i\sigma}$) creates (annihilates) a fermion with spin $\sigma = \uparrow, \downarrow$ at site i of a honeycomb lattice. The first term in Eq. (1) describes nearest-neighbor hopping of amplitude t . The second term defines an interaction on a hexagonal plaquette between next-nearest-neighbor pairs of sites $\langle\langle i,j \rangle\rangle$ (see inset of Fig. 1) with $\hat{J}_{i,j} = i\nu_{ij} \hat{c}_i^\dagger \boldsymbol{\sigma} \hat{c}_j + \text{H.c.}$, $\hat{c}_i^\dagger = (\hat{c}_{i,\uparrow}^\dagger, \hat{c}_{i,\downarrow}^\dagger)$, the Pauli vector $\boldsymbol{\sigma} = (\sigma^x, \sigma^y, \sigma^z)$, and phase factors $\nu_{ij} = \pm 1$ as in the Kane-Mele model [16, 17]. The last term is an attractive, onsite Hubbard interaction ($U > 0$) with $\hat{n}_{i\sigma} \equiv \hat{c}_{i,\sigma}^\dagger \hat{c}_{i,\sigma}$, see Fig. 1. In addition to the global $SU(2) \times U(1)$ symmetry discussed above, \hat{H} is invariant under a particle-hole transformation so that our choice of chemical potential $\mu = 0$ corresponds to half-filling ($\langle \hat{n}_{i\sigma} \rangle = 1/2$).

Hamiltonian (1) was simulated using the ALF (Algorithms for Lattice Fermions) implementation [18, 19] of the grand-canonical, finite-temperature, auxiliary-field QMC method [20, 21]. A sign problem is absent since, after a Hubbard-Stratonovitch transformation to decouple the perfect square interaction terms, time-reversal symmetry as well as $U(1)$ charge conservation are present for each field configuration [22]. Results were obtained on lattices with $L \times L$ unit cells ($2L^2$ sites) and periodic boundary conditions. We use units where $\hbar = k_B = t = 1$ and set $\Delta\tau = 0.2$ for the Trotter discretization.

Phase diagram.—To determine the phase boundaries, we computed the susceptibilities of operators of spin-orbit coupling, $\hat{O}_{\mathbf{r},\delta}^{\text{QSHI}} = i\hat{c}_{\mathbf{r},\delta}^\dagger \boldsymbol{\sigma} \hat{c}_{\mathbf{r}+\delta} + \text{H.c.}$, and on-site s-wave pairing, $\hat{O}_{\mathbf{r},\delta}^{\text{SSC}} = \frac{1}{2} \hat{c}_{\mathbf{r}+\delta,\uparrow}^\dagger \hat{c}_{\mathbf{r}+\delta,\downarrow}^\dagger + \text{H.c.}$ Here, \mathbf{r} specifies a unit cell containing A and B orbitals as well as a hexagon, $\mathbf{r} + \delta$ runs over hexagon, and $\mathbf{r} + \tilde{\delta}$ over the two orbitals of the unit cell. The susceptibilities read

$$\chi_{\delta,\delta'}^\alpha(\mathbf{q}) = \frac{1}{L^2} \sum_{\mathbf{r},\mathbf{r}'} \int_0^\beta d\tau e^{i\mathbf{q}\cdot(\mathbf{r}-\mathbf{r}')} \langle \hat{O}_{\mathbf{r},\delta}^\alpha(\tau) \hat{O}_{\mathbf{r}',\delta'}^\alpha(0) \rangle$$

with $\beta = 1/T$ and $\alpha = \text{QSHI, SSC}$. After diagonalizing

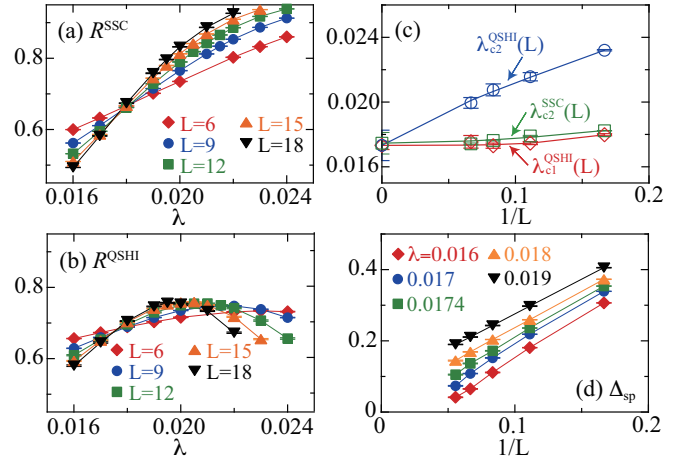


FIG. 2. Correlation ratios for (a) SSC order and (b) QSHI order at $U = 0.4$ for different L and $\beta = L$. Extrapolation of the crossing points of results for L and $L + 3$ in (c) yields a single critical point at $\lambda_c \approx 0.0174$. (d) Single-particle gap at the Dirac point $\mathbf{q} = \mathbf{K}$ near λ_c at $U = 0.4$. Here, $T = 1/30$, representative of the ground state for the parameters shown.

the matrices $\chi_{\delta,\delta'}^\alpha(\mathbf{q})$, we extracted the renormalization-group invariant correlation ratios [23, 24]

$$R^\alpha = 1 - \frac{\chi^\alpha(\mathbf{q}_0 + \delta\mathbf{q})}{\chi^\alpha(\mathbf{q}_0)}. \quad (2)$$

Here, $\chi^\alpha(\mathbf{q})$ is the largest eigenvalue of $\chi_{\delta,\delta'}^\alpha(\mathbf{q})$, \mathbf{q}_0 the ordering wave vector, and $\mathbf{q}_0 + \delta\mathbf{q}$ the longest wave-length fluctuation of the ordered state for a given lattice size. Long-range order in channel α implies a divergent corresponding susceptibility $\chi^\alpha \equiv \chi^\alpha(\mathbf{q}_0 = 0)$. Accordingly, $R^\alpha \rightarrow 1$ for $L \rightarrow \infty$, whereas $R^\alpha \rightarrow 0$ in the disordered phase. At the critical point, R^α becomes scale-invariant for sufficiently large system size L , leading to a crossing of results for different L . We assumed a dynamical critical exponent $z = 1$ to set $L = \beta$ in the finite-size scaling, as justified by the emergent Lorentz invariance of the corresponding field theory [12, 14, 25].

Figure 1 shows the resulting ground-state phase diagram in the λ - U plane. Previous work at $U = 0$ revealed consecutive DSM-QSHI and QSHI-SSC quantum phase transitions with increasing λ [17, 26]. In particular, the DSM is stable up to a nonzero critical interaction due to its vanishing density of states [27]. The DSM-QSHI transition is an example of a Gross-Neveu critical point [12], whereas the QSHI-SSC transition can be understood in the framework of DQCPs [28]. We find that the additional Hubbard interaction favors SSC order, reducing the extent of the QSHI phase with increasing U . For $U \gtrsim 0.5$, we observe a direct DSM-SSC transition with increasing λ that is expected to be in the previously studied $U(1)$ Gross-Neveu universality class [29, 30] (see the SM [31]). A key feature of the phase diagram of Hamiltonian (1) is the existence (within our accuracy) of a

multicritical point at which the DSM, QSHI, and SSC phases meet.

Detailed results for $U = 0.4$ are presented in Fig. 2. The data for R^{SSC} in Fig. 2(a) are consistent with a transition to the SSC phase at $\lambda_{c2}^{\text{SSC}} = 0.0174(6)$, the value obtained by extrapolating the crossing points to $L \rightarrow \infty$ in Fig. 2(c). The analysis of R^{QSHI} at $U = 0.4$ is more involved. Figure 2(b) suggests two phase transitions and an intermediate QSHI phase, as observed for smaller U . However, the extrapolation of the two sets of crossing points, shown in Fig. 2(c), reveals a single transition at the same value, $\lambda_{c1}^{\text{QSHI}} = 0.0174(2)$ and $\lambda_{c2}^{\text{QSHI}} = 0.0174(8)$, and hence a multicritical point at $(\lambda_c, U_c) \approx (0.0174, 0.4)$. At this point, according to Fig. 2(d), the single-particle gap vanishes. The latter was extracted from the asymptotic behavior of the imaginary-time single-particle Green function [32]. Evidence for a continuous transition in terms of the free-energy derivative as well as results for other values of U can be found in [31].

Multicritical point.—We now turn to the nature of the multicritical point. A possible field-theory description is based on a 16-component spinor $\hat{\Psi}_{\nu,\mu,\tau,\sigma}^\dagger(\mathbf{k})$ with Bogoliubov (ν), valley (μ), orbital (τ), and spin (σ) indices. Specifically, $\hat{\Psi}_{1,\mu,\tau,\sigma}^\dagger(\mathbf{k}) = \hat{c}_{\tau,\mu\mathbf{K}+\mathbf{k},\sigma}^\dagger$ and $\hat{\Psi}_{-1,\mu,\tau,\sigma}^\dagger(\mathbf{k}) = \hat{c}_{\tau,\mu\mathbf{K}-\mathbf{k},\sigma}^\dagger$, with the Dirac points $\pm\mathbf{K}$. In this basis, the Dirac Hamiltonian reads

$$\hat{H}_0 = -\frac{v_F}{2} \sum_{\mathbf{k}} \hat{\Psi}^\dagger(\mathbf{k}) (k_x \tau^x \mu^z - k_y \nu^z \tau^y) \hat{\Psi}(\mathbf{k}), \quad (3)$$

where the Pauli matrix τ^α acts on τ and likewise for the other indices. The ordered phases observed numerically correspond to five mutually anti-commuting mass terms \hat{M}_i . For instance, the three QSHI mass terms read $\hat{M}^{\text{QSHI}} = \sum_{\mathbf{k}} \hat{\Psi}^\dagger(\nu^z \sigma^x, \sigma^y, \nu^z \sigma^z) \mu^z \tau^z \hat{\Psi}$ and the two SSC masses are given by $\hat{M}^{\text{SSC}} = \sum_{\mathbf{k}} \hat{\Psi}^\dagger(\nu^y, \nu^x) \sigma^y \mu^x \hat{\Psi}$. The Gross-Neveu Lagrangian expected to describe the multicritical point is

$$\mathcal{L} = \mathcal{L}_0 + g\varphi(\mathbf{x}) \cdot \mathbf{M}(\mathbf{x}) + \mathcal{L}_B(\varphi), \quad (4)$$

where $\varphi(\mathbf{x})$ is a five-component field at a point \mathbf{x} in 2+1D Euclidean space, \mathcal{L}_0 is the Lagrangian density of the free Dirac system and $\mathcal{L}_B(\varphi)$ that of the bosonic field. Both, \mathcal{L}_0 and $g\varphi(\mathbf{x}) \cdot \mathbf{M}(\mathbf{x})$ are invariant under $\text{SO}(5)$ rotations generated by $\frac{i}{2}[\hat{M}_i, \hat{M}_j]$. However, $\mathcal{L}_B(\varphi)$ is only invariant under the $\text{SO}(3) \times \text{SO}(2)$ rotation of the order parameter vector.

Based on an ϵ -expansion, it is argued in Ref. [7] that the terms that reduce the symmetry from $\text{SO}(5)$ to $\text{SO}(3) \times \text{SO}(2)$ are irrelevant at the multicritical point. To obtain numerical evidence, we consider the generator of $\text{SO}(5)$ that rotates between QSHI and SSC order, given by $\frac{i}{2}[\hat{M}_z^{\text{QSHI}}, \hat{M}_1^{\text{SSC}}]$. A lattice realization of this

operator takes the form $\hat{\pi} = \sum_{\mathbf{r}} \hat{\pi}_{\mathbf{r}}$ with [31]

$$\begin{aligned} \hat{\pi}_{\mathbf{r}} = & \hat{a}_{\mathbf{r}}^\dagger \sigma^x \hat{a}_{\mathbf{r}+\mathbf{a}_1}^\dagger + \hat{a}_{\mathbf{r}+\mathbf{a}_1}^\dagger \sigma^x \hat{a}_{\mathbf{r}+\mathbf{a}_2}^\dagger + \hat{a}_{\mathbf{r}+\mathbf{a}_2}^\dagger \sigma^x \hat{a}_{\mathbf{r}}^\dagger \\ & - \hat{b}_{\mathbf{r}}^\dagger \sigma^x \hat{b}_{\mathbf{r}+\mathbf{a}_1}^\dagger - \hat{b}_{\mathbf{r}+\mathbf{a}_1}^\dagger \sigma^x \hat{b}_{\mathbf{r}+\mathbf{a}_2}^\dagger - \hat{b}_{\mathbf{r}+\mathbf{a}_2}^\dagger \sigma^x \hat{b}_{\mathbf{r}}^\dagger + \text{H.c.} \end{aligned} \quad (5)$$

Here, $\hat{a}_{\mathbf{r}}^\dagger = (\hat{a}_{\mathbf{r},\uparrow}^\dagger, \hat{a}_{\mathbf{r},\downarrow}^\dagger)$ and $\hat{a}_{\mathbf{r},\sigma}^\dagger$ creates an electron in orbital A of unit cell \mathbf{r} ; a similar definition holds for $\hat{b}_{\mathbf{r}}^\dagger$. The operator $\hat{\pi}$ transforms as the z -component of a vector under spin rotations. It is odd under inversion and time reversal [31] and breaks the $U(1)$ charge symmetry. Our use of the same notation as in the $\text{SO}(5)$ theory of high-temperature superconductivity [6] is motivated by an expected resonance in neutron scattering experiments at the antiferromagnetic wave vector (π, π) (being odd under inversion) inside the SSC phase with broken $U(1)$ symmetry.

In Fig. 3(a), we plot QMC results for $C^\pi(\tau) = \langle \hat{\pi}(\tau) \hat{\pi}(0) \rangle$ at $(\lambda, U) = (0.0174, 0.4)$, the estimated location of the multicritical point. The fact that $C^\pi(\tau)$ is independent of τ at large τ has important implications. The time τ_1 beyond which $C^\pi(\tau) \approx \text{const.}$ defines an energy scale $\Lambda = \frac{1}{\tau_1}$ as well as a projection onto a low-energy Hilbert space, $\hat{P} = \sum_{E_n - E_0 < \Lambda} |n\rangle \langle n|$ with $\hat{H}|n\rangle = E_n|n\rangle$. In the latter, the τ -independence of $C^\pi(\tau)$ is equivalent to the statement that $\hat{P}[\hat{H}, \hat{\pi}]\hat{P} = 0$ [31]. Precisely the same holds for a conserved quantity such as the total charge at the UV scale. In this case, τ_1 vanishes and the Hamiltonian commutes with the total particle number. From these arguments and the data in Fig. 3(a), we infer that $\hat{\pi}$ commutes with the low-energy

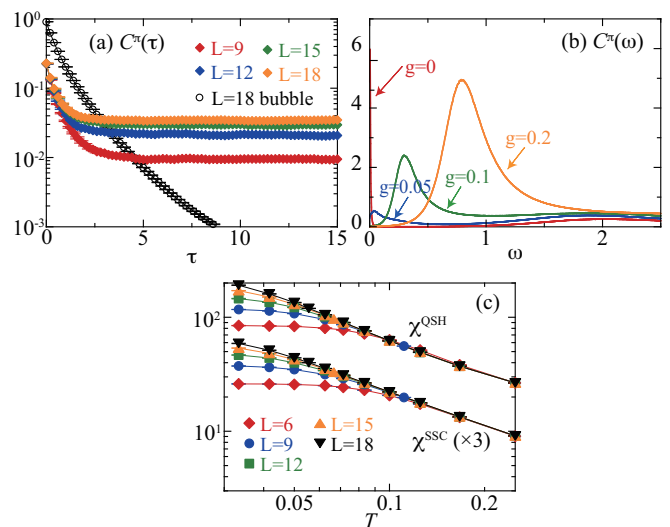


FIG. 3. (a) Time-displaced correlation function of $\hat{\pi}$, $C^\pi(\tau)$, at the multicritical point ($U = 0.4$, $\lambda = 0.0174$) for $T = 1/30$. Also shown is the result of a bubble calculation. (b) Dynamical structure factor $C^\pi(\omega)$ along the dashed line in Fig. 1. Here, $T = 1/30$ and $L = 18$. (c) Temperature dependence of the QSHI and SSC susceptibilities at $U = 0.4$, $\lambda = 0.0174$.

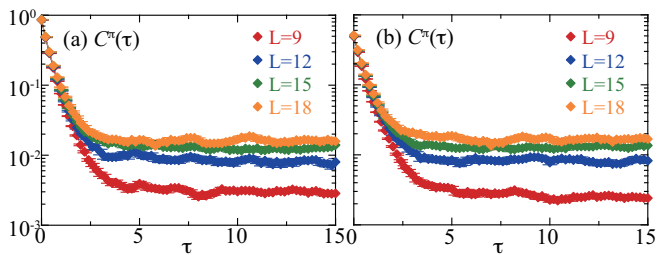


FIG. 4. Time-displaced correlation function $C^\pi(\tau)$ at the DQCP for (a) $U = 0$ and (b) $U = 0.2$. Here, $T = 1/30$.

effective Hamiltonian, $\hat{H}_{\text{eff}} = \hat{P}\hat{H}\hat{P}$. This in turn implies an emergent $\text{SO}(5)$ symmetry.

Figure 3(a) also includes results obtained by neglecting vertex contributions. This *bubble* approximation to $C^\pi(\tau)$ exhibits a clear decay even at large τ , revealing that our findings are linked to interactions in the particle-particle channel.

Because the π mode carries charge and spin, it is expected to acquire an energy gap both in the QSHI and the spin-singlet SSC phases. This can be verified by considering the corresponding dynamical structure factor, $C^\pi(\omega) = \text{Im}\chi(\omega)/(1 - e^{-\beta\omega})$ with $\chi(\omega) = i \int_0^\infty dt e^{i\omega t} \langle [\hat{\pi}, \hat{\pi}(-t)] \rangle$. We computed this quantity using stochastic analytical continuation [33], as implemented in the ALF [19] library. The results in Fig. 3(b) are for different path distances g from the multicritical point along the path shown in Fig. 1. They confirm that the π mode is gapless at criticality ($g = 0$) but has a gap that increases with g as we go deeper into the SSC phase.

Further evidence for an emergent $\text{SO}(5)$ symmetry can be obtained from the temperature dependence of the QSHI and SSC susceptibilities. At the multicritical point, and given Lorentz invariance, they are expected to scale as $\chi^\alpha \sim L^{(2-\eta^\alpha)} f(\beta/L)$, with anomalous dimensions η^α [34]. This is borne out by the QMC results in Fig. 3(c), which exhibit similar behavior at low temperatures and identical values of η within error bars, namely $\eta^{\text{QSHI}} = 0.99(3)$ and $\eta^{\text{SSC}} = 1.01(1)$.

DQCP.—Contrary to the multicritical point, fermionic excitations are gapped at the DQCP. In the framework of Eq. (4), this implies that $|\varphi|$ remains finite and only its phase fluctuations need to be considered. Integrating out the fermions [10, 13] then yields a 2+1D non-linear sigma model with a Wess-Zumino-Witten term that accounts for the phase dynamics of $\varphi/|\varphi|$. The relevance of terms in the field theory that break down the $\text{SO}(5)$ symmetry to $\text{SO}(3) \times \text{U}(1)$ at the critical point can again be addressed using $C^\pi(\tau)$. The results in Fig. 4 were obtained at different values of U . As for the multicritical point, they suggest an emergent $\text{SO}(5)$ symmetry.

Discussion.—The key result our work is the phase diagram (Fig. 1) with a fermionic DSM-QSHI-SSC multicritical point as well as a (bosonic) QSHI-SSC DQCP. Up

to the system size accessible in our simulations, we find that the operator $\hat{\pi}$ that rotates between QSHI and SSC order is a constant of motion of the low-energy effective Hamiltonian at the critical points. This implies identical anomalous dimensions in the QSHI and SSC channels, as verified here at the multicritical point and previously at the DQCP [17]. The substantially different values at the DQCP ($\eta^\alpha \simeq 0.25$ [17] vs. $\eta^\alpha \simeq 1$) exclude the possibility that the results at the latter are due to proximity to the multicritical point. According to Noether's theorem, $\hat{\pi}$ is the zeroth component of a conserved current. Being a conserved quantity, it cannot acquire an anomalous dimension. Such a criterion has been used to detect emergent $\text{SO}(4)$ symmetry in Ref. [35].

Our findings for the multicritical point give numerical confirmation of predictions of an emergent $\text{SO}(5)$ symmetry based on one-loop RG calculations [7, 36]. Although we can provide roughly the same quality of results for the DQCP case, some care has to be taken in interpreting the results for the latter. Enhanced $\text{SO}(4)$ [35, 37, 38] or $\text{SO}(5)$ [39, 40] symmetries have been observed at critical points in various models. In the $\text{SO}(4)$ case, the transition is argued to be of first order [37]. Emergent symmetries can occur at first-order transitions due to fine-tuning. For instance, the spin-flop transition in an $\text{SO}(3)$ symmetric Heisenberg model has $\text{SO}(3)$ symmetry at the UV scale at the transition point. For weakly first-order transitions [38, 41, 42], we can understand emergent symmetries within the RG framework. In this case, the RG flow becomes very slow [40] when approaching the transition. If the operators that break an emergent symmetry have a large scaling dimension, they will be suppressed at intermediate length scales. Therefore, first-order transitions can be naturally reconciled with emergent symmetries without invoking fine-tuning.

The authors gratefully acknowledge the Gauss Centre for Supercomputing e.V. for funding this project by providing computing time on the GCS Supercomputer SUPERMUC-NG at Leibniz Supercomputing Centre. T.S. acknowledges funding from the Deutsche Forschungsgemeinschaft under Grant No. SA 3986/1-1. F.F.A. acknowledges the DFG for funding via Würzburg-Dresden Cluster of Excellence on Complexity and Topology in Quantum Matter ct.qmat (EXC 2147, Project ID 390858490) as well as the SFB1170 on Topological and Correlated Electronics at Surfaces and Interfaces. Y.L. was supported by the National Natural Science Foundation of China under grant No. 11947232. D.H. and W.G. were supported by the National Natural Science Foundation of China under grants No. 12175015 and No. 11734002.

-
- [1] N. Goldenfeld, *Lectures on Phase Transitions and the Renormalization Group (1st ed.)* (CRC Press, (1992)).
- [2] T. Giamarchi, *Quantum physics in one dimension* (Clarendon Press, Oxford, 2004) ISBN 0 19 85 25 00 1.
- [3] J. Manuel Carmona, A. Pelissetto, and E. Vicari, *Phys. Rev. B* **61**, 15136 (2000).
- [4] P. Calabrese, A. Pelissetto, and E. Vicari, *Phys. Rev. B* **67**, 054505 (2003).
- [5] H. Shao, W. Guo, and A. W. Sandvik, *Phys. Rev. Lett.* **124**, 080602 (2020).
- [6] S.-C. Zhang, *Science* **275**, 1089 (1997).
- [7] L. Janssen, I. F. Herbut, and M. M. Scherer, *Phys. Rev. B* **97**, 041117 (2018).
- [8] A. H. C. Neto, F. Guinea, N. M. R. Peres, K. S. Novoselov, and A. K. Geim, *Rev. Mod. Phys.* **81**, 109 (2009).
- [9] S. Ryu, C. Mudry, C.-Y. Hou, and C. Chamon, *Phys. Rev. B* **80**, 205319 (2009).
- [10] A. Tanaka and X. Hu, *Phys. Rev. Lett.* **95**, 036402 (2005).
- [11] Z. Wang, M. P. Zaletel, R. S. K. Mong, and F. F. Assaad, *Phys. Rev. Lett.* **126**, 045701 (2021).
- [12] I. F. Herbut, V. Juričić, and B. Roy, *Phys. Rev. B* **79**, 085116 (2009).
- [13] A. Abanov and P. Wiegmann, *Nuclear Physics B* **570**, 685 (2000).
- [14] T. Senthil, A. Vishwanath, L. Balents, S. Sachdev, and M. P. A. Fisher, *Science* **303**, 1490 (2004).
- [15] T. Senthil and M. P. A. Fisher, *Phys. Rev. B* **74**, 064405 (2006).
- [16] C. L. Kane and E. J. Mele, *Phys. Rev. Lett.* **95**, 146802 (2005).
- [17] Y. Liu, Z. Wang, T. Sato, M. Hohenadler, C. Wang, W. Guo, and F. F. Assaad, *Nature Communications* **10**, 2658 (2019).
- [18] M. Bercx, F. Goth, J. S. Hofmann, and F. F. Assaad, *SciPost Phys.* **3**, 013 (2017).
- [19] F. F. Assaad, M. Bercx, F. Goth, A. Götz, J. S. Hofmann, E. Huffman, Z. Liu, F. P. Toldin, J. S. E. Portela, and J. Schwab, *SciPost Phys. Codebases*, 1 (2022).
- [20] R. Blankenbecler, D. J. Scalapino, and R. L. Sugar, *Phys. Rev. D* **24**, 2278 (1981).
- [21] F. Assaad and H. Evertz, in *Computational Many-Particle Physics*, Lecture Notes in Physics, Vol. 739, edited by H. Fehske, R. Schneider, and A. Weiße (Springer, Berlin Heidelberg, 2008) pp. 277–356.
- [22] C. Wu and S.-C. Zhang, *Phys. Rev. B* **71**, 155115 (2005).
- [23] K. Binder, *Z. Phys. B Con. Mat.* **43**, 119 (1981).
- [24] S. Pujari, T. C. Lang, G. Murthy, and R. K. Kaul, *Phys. Rev. Lett.* **117**, 086404 (2016).
- [25] D. J. Gross and A. Neveu, *Phys. Rev. D* **10**, 3235 (1974).
- [26] Y. Liu, Z. Wang, T. Sato, W. Guo, and F. F. Assaad, *Phys. Rev. B* **104**, 035107 (2021).
- [27] S. Sorella and E. Tosatti, *Europhysics Letters* **19**, 699 (1992).
- [28] T. Senthil, L. Balents, S. Sachdev, A. Vishwanath, and M. P. A. Fisher, *Phys. Rev. B* **70**, 144407 (2004).
- [29] Z.-X. Li, Y.-F. Jiang, S.-K. Jian, and H. Yao, *Nature Communications* **8**, 314 (2017).
- [30] Y. Otsuka, K. Seki, S. Sorella, and S. Yunoki, *Phys. Rev. B* **98**, 035126 (2018).
- [31] See Supplemental Material [URL] for additional data and technical details.
- [32] F. F. Assaad and M. Imada, *J. Phys. Soc. Jpn.* **65**, 189 (1996).
- [33] K. S. D. Beach, eprint arXiv:cond-mat/0403055 (2004), cond-mat/0403055.
- [34] M. Campostrini, A. Pelissetto, and E. Vicari, *Phys. Rev. B* **89**, 094516 (2014).
- [35] N. Ma, Y.-Z. You, and Z. Y. Meng, *Phys. Rev. Lett.* **122**, 175701 (2019).
- [36] B. Roy, P. Goswami, and V. Juričić, *Phys. Rev. B* **97**, 205117 (2018).
- [37] B. Zhao, P. Weinberg, and A. W. Sandvik, *Nature Physics* **15**, 678 (2019).
- [38] T. Sato, M. Hohenadler, and F. F. Assaad, *Phys. Rev. Lett.* **119**, 197203 (2017).
- [39] A. Nahum, P. Serna, J. T. Chalker, M. Ortuño, and A. M. Somoza, *Phys. Rev. Lett.* **115**, 267203 (2015).
- [40] A. Nahum, J. T. Chalker, P. Serna, M. Ortuño, and A. M. Somoza, *Phys. Rev. X* **5**, 041048 (2015).
- [41] E. Torres, L. Weber, L. Janssen, S. Wessel, and M. M. Scherer, *Phys. Rev. Research* **2**, 022005 (2020).
- [42] J. Zhao, Y.-C. Wang, Z. Yan, M. Cheng, and Z. Y. Meng, *Phys. Rev. Lett.* **128**, 010601 (2022).

SUPPLEMENTAL MATERIAL

FREE-ENERGY DERIVATIVE AND SSC-QSHI SUSCEPTIBILITY RATIO

In the main text, we discuss a multicritical point with an emergent SO(5) symmetry at which DSM, QSHI, and SSC phases meet. The scaling behavior observed in Fig. 2 is consistent with a continuous phase transition. This can be substantiated by calculating the free-energy derivative

$$\frac{\partial F}{\partial \lambda} = -\frac{1}{L^2} \left\langle \sum_{\square} \left(\sum_{\langle\langle i,j \rangle\rangle \in \square} \hat{J}_{i,j} \right)^2 \right\rangle, \quad (6)$$

which shows no sign of a discontinuity [Fig. 5(a)].

To verify whether the multicritical point has an emergent SO(5) symmetry, we also measured the ratio of the QSHI and SSC susceptibilities χ^α . These quantities are in general independent but become locked together and can be combined into a five-component order parameter if a unifying SO(5) symmetry emerges. In this case, the ratio $\chi^{\text{SSC}}/\chi^{\text{QSHI}}$ is expected to become scale invariant, consistent with the data in Fig. 5(b).

FINITE-SIZE SCALING AT THE GROSS-NEVEU AND DECONFINED CRITICAL POINTS

The phase boundaries in Fig. 1 are based on results for the correlation ratios R^{SSC} and R^{QSHI} . Here, we present typical results for the DSM-QSHI and DSM-SSC Gross-Neveu transitions as well as for the QSHI-SSC DQCP.

Figures 6(a)–6(c) show results for $U = 0.2$. The data for R^{SSC} in Fig. 6(a) are consistent with a DSM-SSC transition at $\lambda_{c2}^{\text{SSC}} = 0.0258(1)$, the value obtained by extrapolating the crossing points to $L \rightarrow \infty$ [Fig. 6(c)]. Figure 6(b) reveals two phase transitions and an intermediate QSHI phase. The extrapolation of the two sets of crossing point in Fig. 6(c) yields $\lambda_{c1}^{\text{QSHI}} = 0.0182(2)$ and $\lambda_{c2}^{\text{QSHI}} = 0.0263(6)$, respectively. Within error bars, $\lambda_{c2}^{\text{SSC}}$ and $\lambda_{c2}^{\text{QSHI}}$ are identical, consistent with a direct QSHI-SSC transition.

In Figs. 6(d)–6(f), we report results at $U = 0.6$. The data for R^{SSC} and R^{QSHI} indicate a single phase transition without an intermediate QSHI phase. The extrapolation of the crossing points [Fig. 6(f)] yields $\lambda_{c2}^{\text{SSC}} = 0.0149(1)$ for the DSM-SSC transition.

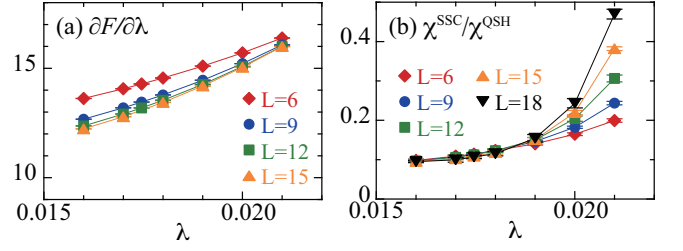


FIG. 5. (a) Free-energy derivative and (b) ratio of QSHI and SSC susceptibilities $\chi^{\text{SSC}}/\chi^{\text{QSHI}}$ close to the multicritical point ($\lambda = 0.0174$, $U = 0.4$). Here, $T = 1/30$, representative of the ground state for the parameters considered.

MASS TERMS AND THE π OPERATOR

In the continuum limit, the tight-binding model on the honeycomb lattice reduces to the Dirac Hamiltonian

$$\hat{H}_0 = -v_F \sum_{\mathbf{k}, \tau, \tau', \mu, \mu', \sigma} \hat{c}_{\tau, \mu \mathbf{K} + \mathbf{k}, \sigma}^\dagger (k_x \tau_{\tau, \tau'}^x \mu_{\mu, \mu'}^z - k_y \tau_{\tau, \tau'}^y \delta_{\mu, \mu'}) \hat{c}_{\tau', \mu' \mathbf{K} + \mathbf{k}, \sigma}. \quad (7)$$

Here, $\mathbf{K} = \frac{4}{3}\mathbf{b}_1 + \frac{4}{3}\mathbf{b}_2$ with \mathbf{b}_i the reciprocal lattice vectors satisfying $\mathbf{b}_i \cdot \mathbf{a}_j = 2\pi\delta_{i,j}$. The Fermi velocity $v_F = \sqrt{3}at/2$ with a the lattice spacing and t the hopping matrix element. The indices τ , μ , and σ refer to orbital, valley, and spin, respectively, and take on values $\{-1, 1\}$. τ^α , μ^α , and σ^α are Pauli matrices satisfying the Clifford algebra, $\{\tau^\alpha, \tau^\beta\} = 2\delta_{\alpha,\beta}$, etc.

In the presence of superconducting mass terms, it is convenient to adopt a Bogoliubov basis

$$\hat{\Psi}_{\nu, \mu, \tau, \sigma}^\dagger(\mathbf{k}) = \begin{cases} \hat{c}_{\tau, \mu \mathbf{K} + \mathbf{k}, \sigma}^\dagger & \text{if } \nu = +1, \\ \hat{c}_{\tau, \mu \mathbf{K} - \mathbf{k}, \sigma} & \text{if } \nu = -1, \end{cases} \quad (8)$$

in which the Hamiltonian takes the form

$$\hat{H}_0 = -\frac{v_F}{2} \sum_{\mathbf{k}, \nu, \nu', \tau, \tau', \mu, \mu', \sigma} \hat{\Psi}_{\nu, \tau, \mu, \sigma}^\dagger(\mathbf{k}) (k_x \delta_{\nu, \nu'} \tau_{\tau, \tau'}^x \mu_{\mu, \mu'}^z - k_y \nu_{\nu, \nu'}^z \tau_{\tau, \tau'}^y \delta_{\mu, \mu'}) \hat{\Psi}_{\nu', \tau', \mu', \sigma}(\mathbf{k}). \quad (9)$$

We introduced another set of Pauli matrices ν^α acting on the Bogoliubov index.

Let us define mass terms as

$$\hat{M} = \sum_{\mathbf{k}} \hat{\Psi}^\dagger(\mathbf{k}) M \hat{\Psi}(\mathbf{k}), \quad (10)$$

where $M = M_{\nu, \nu', \tau, \tau', \mu, \mu', \sigma, \sigma'}$ is a 16×16 matrix accounting for the Bogoliubov, valley, orbital, and spin indices. In this basis, the three QSHI mass terms read

$$\begin{aligned} M_x^{\text{QSHI}} &= \nu^z \sigma^x \mu^z \tau^z, \\ M_y^{\text{QSHI}} &= \sigma^y \mu^z \tau^z, \\ M_z^{\text{QSHI}} &= \nu^z \sigma^z \mu^z \tau^z. \end{aligned} \quad (11)$$

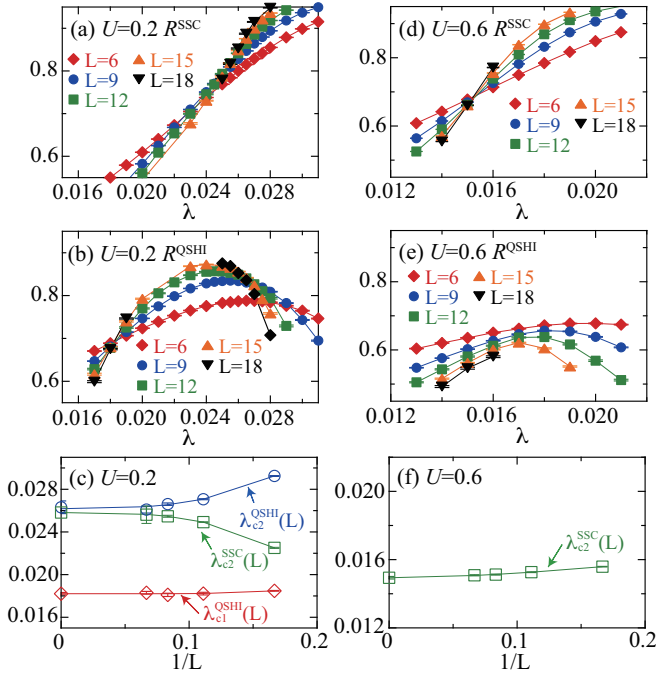


FIG. 6. Correlation ratios R^{SSC} [(a),(d)] and R^{QSHI} [(b),(e)] for different system sizes L at fixed $\beta = L$. Extrapolation of the crossing points $\lambda_{c1}^\alpha(L)$ and $\lambda_{c2}^\alpha(L)$ between curves for L and $L + 3$ gives the critical values reported in Fig. 1 [(c),(f)].

The two SC masses, corresponding to the real and imaginary parts of the SSC order parameter, are

$$\begin{aligned} M_1^{\text{SSC}} &= \nu^y \sigma^y \mu^x, \\ M_2^{\text{SSC}} &= \nu^x \sigma^y \mu^x. \end{aligned} \quad (12)$$

By definition, these mass terms anti-commute with \hat{H}_0 and mutually anti-commute.

We are now in a position to compute the modes that rotate between QSHI and SSC order. We focus on

$$\Pi = \frac{i}{2} [M_1^{\text{SSC}}, M_z^{\text{QSHI}}] = -\nu^x \sigma^x \mu^y \tau^z. \quad (13)$$

The corresponding operator is given by

$$\hat{\Pi} = -2i \sum_{\substack{\mathbf{k}, \tau, \tau' \\ \sigma, \sigma'}} \hat{c}_{\tau, -\mathbf{K} - \mathbf{k}, \sigma}^\dagger \sigma_{\sigma, \sigma'}^x \tau_{\tau, \tau'}^z \hat{c}_{\tau', \mathbf{K} + \mathbf{k}, \sigma'}^\dagger + \text{H.c.} \quad (14)$$

A regularization on the honeycomb lattice takes the form given in Eq. (5), $\hat{\pi} = \sum_{\mathbf{r}} \hat{\pi}_{\mathbf{r}}$ with

$$\hat{\pi}_{\mathbf{r}} = \hat{a}_{\mathbf{r}}^\dagger \sigma^x \hat{a}_{\mathbf{r} + \mathbf{a}_1}^\dagger + \hat{a}_{\mathbf{r} + \mathbf{a}_1}^\dagger \sigma^x \hat{a}_{\mathbf{r} + \mathbf{a}_2}^\dagger + \hat{a}_{\mathbf{r} + \mathbf{a}_2}^\dagger \sigma^x \hat{a}_{\mathbf{r}}^\dagger - \hat{b}_{\mathbf{r}}^\dagger \sigma^x \hat{b}_{\mathbf{r} + \mathbf{a}_1}^\dagger + \hat{b}_{\mathbf{r} + \mathbf{a}_1}^\dagger \sigma^x \hat{b}_{\mathbf{r} + \mathbf{a}_2}^\dagger + \hat{b}_{\mathbf{r} + \mathbf{a}_2}^\dagger \sigma^x \hat{b}_{\mathbf{r}}^\dagger + \text{H.c.} \quad (15)$$

Here, $\hat{\mathbf{a}}_{\mathbf{r}}^\dagger = (\hat{a}_{\mathbf{r}, \uparrow}^\dagger, \hat{a}_{\mathbf{r}, \downarrow}^\dagger)$ and $\hat{\mathbf{b}}_{\mathbf{r}}^\dagger = (\hat{b}_{\mathbf{r}, \uparrow}^\dagger, \hat{b}_{\mathbf{r}, \downarrow}^\dagger)$. The operators $\hat{a}_{\mathbf{r}, \sigma}^\dagger$ and $\hat{b}_{\mathbf{r}, \sigma}^\dagger$ create fermions in the A and B orbitals of unit cell \mathbf{r} , respectively; $\mathbf{a}_1 = a(1, 0)$ and $\mathbf{a}_2 = a(1/2, \sqrt{3}/2)$ are the basis vectors.

We now discuss the symmetry properties of $\hat{\Pi}$.

Time reversal: Since the SSC and QSHI mass terms are even under time reversal, $\hat{\Pi}$ has to be odd. This becomes apparent from Eq. (15) since σ_x maps onto $-\sigma_x$ under time reversal.

Inversion: Inversion around the center of a hexagon leaves the SSC order parameter invariant. On the other hand, the QSHI order parameters are odd under this operation. Hence, $\hat{\Pi}$ is odd under inversion. Accordingly, in Eq. (15), interchanging $\hat{\mathbf{a}}$ and $\hat{\mathbf{b}}$ flips the sign of $\hat{\pi}_{\mathbf{r}}$.

Spin rotations: To understand spin rotations, we note that defining

$$U(\mathbf{e}, \theta) = e^{-i\theta \mathbf{e} \cdot \boldsymbol{\sigma} / 2} \quad (16)$$

we have

$$\begin{aligned} U^\dagger(\mathbf{e}, \theta) \boldsymbol{\sigma} \sigma_y [U^\dagger(\mathbf{e}, \theta)]^T &= U^\dagger(\mathbf{e}, \theta) \boldsymbol{\sigma} U(\mathbf{e}, \theta) \sigma_y \\ &= R(\mathbf{e}, \theta) \boldsymbol{\sigma} \sigma_y \end{aligned} \quad (17)$$

with $R(\mathbf{e}, \theta)$ an SO(3) rotation around axis \mathbf{e} with angle θ . Using Eq. (17), it can be verified that the SSC mass term is a spin singlet and hence invariant under the transformation: $\hat{c}_{\tau, \mu \mathbf{K} + \mathbf{k}, \sigma} \rightarrow \sum_{\sigma'} U(\mathbf{e}, \theta)_{\sigma, \sigma'} \hat{c}_{\tau, \mu \mathbf{K} + \mathbf{k}, \sigma'}$. On the other hand, the QSHI mass terms transform as a vector, $\hat{M}^{\text{QSHI}} \rightarrow R(\mathbf{e}, \theta) \hat{M}^{\text{QSHI}}$. Writing $\sigma^x = \mathbf{e}^z \cdot \boldsymbol{\sigma} i \sigma^y$, it becomes apparent that $\hat{\pi}$ transforms as the z -component of the QSHI masses.

τ -INDEPENDENCE OF $C^\pi(\tau)$ AND EMERGENT SYMMETRY

Consider the energy basis representation, $\hat{H}|n, \lambda_n\rangle = E_n|n, \lambda_n\rangle$. Here, we allow for degeneracies λ_n of the energy eigenstates. In this basis, time-displaced correlation functions of a hermitian operator read

$$\langle \hat{O}(\tau) \hat{O} \rangle = \frac{\sum_{n, \lambda_n, m, \lambda_m} e^{-\beta E_n} e^{\tau[E_n - E_m]} |\langle n, \lambda_n | \hat{O} | m, \lambda_m \rangle|^2}{\sum_{n, \lambda_n} e^{-\beta E_n}}. \quad (18)$$

We will assume that for $\tau > \tau_1$, with $0 < \tau_1 < \beta/2$, the correlation function is constant up to exponentially

small corrections and set $E_0 = 0$. Then, $1/\Lambda = \min(\beta - \tau_1, \tau_1)$ defines an inverse energy scale. We can define a projection onto a low-energy Hilbert space,

$$\hat{P} = \sum_{n, \lambda_n, E_n < \Lambda} |n, \lambda_n\rangle \langle n, \lambda_n|, \quad (19)$$

and a low-energy effective Hamiltonian,

$$\hat{H}_{\text{eff}} = \hat{P} \hat{H} \hat{P}. \quad (20)$$

Following our initial assumption,

$$\langle \hat{O}(\tau) \hat{O} \rangle_{\text{eff}} = \frac{\text{Tr} \left[\hat{P} e^{-(\beta-\tau)\hat{H}} \hat{O} \hat{P} e^{-\tau\hat{H}} \hat{O} \right]}{\text{Tr} \left[\hat{P} e^{-\beta\hat{H}} \right]} \quad (21)$$

does not depend on τ .

As a consequence of Eq. (18), and for energy eigenstates in the low-energy Hilbert space, $\hat{O}|m, \lambda_m\rangle$ has to be included in the eigenspace \mathcal{H}_{E_m} of the E_m eigenvalue: $\{|m, \lambda_m\rangle, \lambda_m = 1 \dots, \dim \mathcal{H}_{E_m}\}$. In other words,

$$\hat{O}|m, \lambda_m\rangle = \sum_{\lambda_{m'}} O_{\lambda_m, \lambda_{m'}} |m, \lambda_{m'}\rangle. \quad (22)$$

We can now perform a unitary transformation in each eigenspace to construct the basis $|\widetilde{m}, \widetilde{\lambda}_m\rangle$ satisfying

$$\begin{aligned} \hat{H}_{\text{eff}} |\widetilde{m}, \widetilde{\lambda}_m\rangle &= E_m |\widetilde{m}, \widetilde{\lambda}_m\rangle, \\ \hat{O} |\widetilde{m}, \widetilde{\lambda}_m\rangle &= O_{m, \lambda_m} |\widetilde{m}, \widetilde{\lambda}_m\rangle. \end{aligned} \quad (23) \quad \text{with}$$

Hence,

$$[\hat{H}_{\text{eff}}, \hat{O}] = 0. \quad (24)$$

Equation (24) implies that $\langle \hat{O}(\tau) \hat{O} \rangle_{\text{eff}} = \langle \hat{O} \hat{O} \rangle_{\text{eff}}$ is τ -independent. For our specific case, the operator $\hat{O} = \hat{\pi}$ transforms as the z -component of a vector under spin rotations. Since \hat{H}_{eff} has the same symmetries as \hat{H} , and assuming that the ground state is a spin singlet, we have $\hat{\pi}|0\rangle = 0$ and $\lim_{\beta \rightarrow \infty} \langle \hat{\pi} \cdot \hat{\pi} \rangle = \|\hat{\pi}|0\rangle\|^2 = 0$. In contrast, at finite temperatures, there is no symmetry argument for $\langle \hat{\pi} \cdot \hat{\pi} \rangle$ to vanish.

BUBBLE APPROXIMATION OF $C^\pi(\tau)$

In the main text, we reported results for the imaginary-time correlation function of $\hat{\pi}$ [Eq. (15)],

$$\begin{aligned} C^\pi(\tau) &= \frac{1}{L^2} \sum_{i,j} \langle \hat{\pi}_i(\tau) \hat{\pi}_j(0) \rangle \\ &= \langle \hat{\pi}_{\mathbf{q}}(\tau) \hat{\pi}_{-\mathbf{q}}(0) \rangle_{\mathbf{q}=0} \end{aligned} \quad (25)$$

$$\begin{aligned} \hat{\pi}_{\mathbf{q}}(\tau) &= \frac{1}{L} \sum_l (-1)^l \sum_{\mathbf{k}} \left[\left(e^{-i(\mathbf{k}-\mathbf{q})\cdot\mathbf{a}_1} + e^{i(\mathbf{k}\cdot\mathbf{a}_1 - (\mathbf{k}-\mathbf{q})\cdot\mathbf{a}_2)} + e^{i\mathbf{k}\cdot\mathbf{a}_2} \right) \hat{c}_{\mathbf{k},l}^\dagger(\tau) \sigma^x \hat{c}_{-\mathbf{k}+\mathbf{q},l}^\dagger(\tau) \right. \\ &\quad \left. + \left(e^{i(\mathbf{k}+\mathbf{q})\cdot\mathbf{a}_1} + e^{-i(\mathbf{k}\cdot\mathbf{a}_1 - (\mathbf{k}+\mathbf{q})\cdot\mathbf{a}_2)} + e^{-i\mathbf{k}\cdot\mathbf{a}_2} \right) \hat{c}_{-\mathbf{k}-\mathbf{q},l}(\tau) \sigma^x \hat{c}_{\mathbf{k},l}(\tau) \right]. \end{aligned} \quad (26)$$

Here, $\hat{c}_{\mathbf{k},l}^\dagger = (\hat{c}_{\mathbf{k},l,\uparrow}^\dagger, \hat{c}_{\mathbf{k},l,\downarrow}^\dagger)$, $l \in \{A, B\}$ is an orbital index and $(-1)^l = 1$ for $l = A$ and -1 for $l = B$.

Using Eqs. (25) and (26), $C^\pi(\tau)$ is given by

$$C^\pi(\tau) = \frac{1}{L^2} \sum_{l,l'} (-1)^{l+l'} \sum_{\mathbf{k},\mathbf{k}'} v_{\mathbf{k}} v_{\mathbf{k}'}^* \left[\langle \hat{c}_{\mathbf{k},l}^\dagger(\tau) \sigma^x \hat{c}_{-\mathbf{k},l}^\dagger(\tau) \hat{c}_{-\mathbf{k}',l'}(0) \sigma^x \hat{c}_{\mathbf{k}',l'}(0) \rangle + \langle \hat{c}_{-\mathbf{k}',l'}(\tau) \sigma^x \hat{c}_{\mathbf{k}',l'}(\tau) \hat{c}_{\mathbf{k},l}^\dagger(0) \sigma^x \hat{c}_{-\mathbf{k},l'}^\dagger(0) \rangle \right] \quad (27)$$

where $v_{\mathbf{k}} = e^{-i\mathbf{k}\cdot\mathbf{a}_1} + e^{i\mathbf{k}\cdot(\mathbf{a}_1 - \mathbf{a}_2)} + e^{i\mathbf{k}\cdot\mathbf{a}_2}$. In the main text, we included results for $C^\pi(\tau)$ that neglect vertex cor-

rections, as calculated from a convolution of the single-particle Green function and

$$\begin{aligned}
C^{0,\pi}(\tau) &= \frac{1}{L^2} \sum_{l,l'} (-1)^{l+l'} \\
&\times \left[\sum_{\mathbf{k}} v_{\mathbf{k}} v_{\mathbf{k}}^* \left(\langle \hat{c}_{\mathbf{k},l,\sigma_1}^\dagger(\tau) \hat{c}_{\mathbf{k},l',\sigma_4}(0) \rangle \langle \hat{c}_{-\mathbf{k},l,\sigma_2}^\dagger(\tau) \hat{c}_{-\mathbf{k},l',\sigma_3}(0) \rangle + \langle \hat{c}_{\mathbf{k},l,\sigma_1}^\dagger(\tau) \hat{c}_{\mathbf{k},l',\sigma_4}^\dagger(0) \rangle \langle \hat{c}_{-\mathbf{k},l,\sigma_2}(\tau) \hat{c}_{-\mathbf{k},l',\sigma_3}^\dagger(0) \rangle \right) \right. \\
&\quad \left. - \sum_{\mathbf{k}} v_{\mathbf{k}} v_{-\mathbf{k}}^* \left(\langle \hat{c}_{\mathbf{k},l,\sigma_1}^\dagger(\tau) \hat{c}_{\mathbf{k},l',\sigma_3}(0) \rangle \langle \hat{c}_{-\mathbf{k},l,\sigma_2}^\dagger(\tau) \hat{c}_{-\mathbf{k},l',\sigma_4}(0) \rangle + \langle \hat{c}_{\mathbf{k},l,\sigma_1}^\dagger(\tau) \hat{c}_{\mathbf{k},l',\sigma_3}^\dagger(0) \rangle \langle \hat{c}_{-\mathbf{k},l,\sigma_2}(\tau) \hat{c}_{-\mathbf{k},l',\sigma_4}^\dagger(0) \rangle \right) \right],
\end{aligned} \tag{28}$$

where $(\sigma_1, \sigma_2, \sigma_3, \sigma_4)$ takes on the values $(\uparrow, \downarrow, \downarrow, \uparrow)$, $(\uparrow, \downarrow, \uparrow, \downarrow)$, $(\downarrow, \uparrow, \uparrow, \downarrow)$, and $(\downarrow, \uparrow, \downarrow, \uparrow)$.